Article

Chemistry & Biology

AMPK Activation via Modulation of De Novo Purine Biosynthesis with an Inhibitor of ATIC Homodimerization

Graphical Abstract

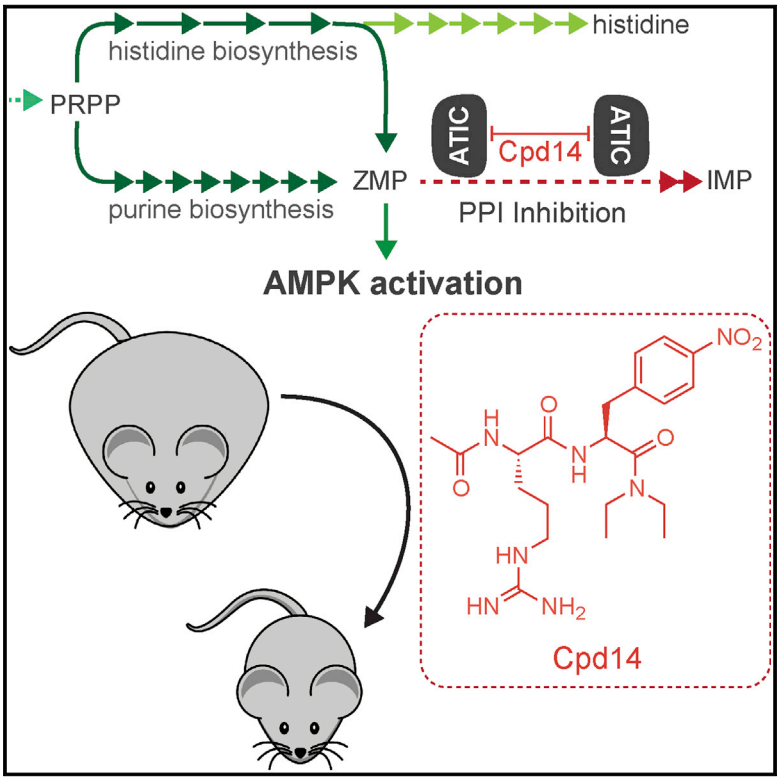

Highlights

- AICAR transformylase is targeted in cells with an ATIC homodimerization inhibitor
- The resulting increase in endogenous ZMP is sufficient to activate AMPK
- Downstream AMPK signaling is also activated, significantly altering cell metabolism
- A mouse model of metabolic syndrome is used to show therapeutic viability

Authors

Daniel J. Asby, Francesco Cuda, Maxime Beyaert, Franchesca D. Houghton, Felino R. Cagampang, Ali Tavassoli

Correspondence

a.tavassoli@soton.ac.uk

In Brief

Asby et al. report a new approach to AMPK activation. Using an inhibitor of AICAR transformylase homodimerization, the ninth step of de novo purine biosynthesis is blocked, causing a rise in endogenous ZMP, which activates AMPK and its downstream effectors.

Asby et al., 2015, Chemistry & Biology 22, 838–848
July 23, 2015
http://dx.doi.org/10.1016/j.chembiol.2015.06.008

CellPress

CellPress

Chemistry & Biology
Article

AMPK Activation via Modulation of De Novo Purine Biosynthesis with an Inhibitor of ATIC Homodimerization

Daniel J. Asby,[1] Francesco Cuda,[1] Maxime Beyaert,[1] Franchesca D. Houghton,[2,3] Felino R. Cagampang,[2,3] and Ali Tavassoli[1,3,*]

[1]Chemistry, University of Southampton, Southampton SO17 1BJ, UK
[2]Human Development and Health, Faculty of Medicine, University of Southampton, Southampton SO16 6YD, UK
[3]The Institute for Life Sciences, University of Southampton, Southampton, UK
*Correspondence: a.tavassoli@soton.ac.uk
http://dx.doi.org/10.1016/j.chembiol.2015.06.008

SUMMARY

5-Aminoimidazole-4-carboxamide ribonucleotide (known as ZMP) is a metabolite produced in de novo purine biosynthesis and histidine biosynthesis, but only utilized in the cell by a homodimeric bifunctional enzyme (called ATIC) that catalyzes the last two steps of de novo purine biosynthesis. ZMP is known to act as an allosteric activator of the cellular energy sensor adenosine monophosphate-activated protein kinase (AMPK), when exogenously administered as the corresponding cell-permeable ribonucleoside. Here, we demonstrate that endogenous ZMP, produced by the aforementioned metabolic pathways, is also capable of activating AMPK. Using an inhibitor of ATIC homodimerization to block the ninth step of de novo purine biosynthesis, we demonstrate that the subsequent increase in endogenous ZMP activates AMPK and its downstream signaling pathways. We go on to illustrate the viability of using this approach to AMPK activation as a therapeutic strategy with an in vivo mouse model for metabolic disorders.

INTRODUCTION

AMP-activated protein kinase (AMPK) is the master regulator of cellular energy homeostasis, monitoring and responding to changes in the intracellular AMP/ATP ratio. AMPK signaling extends through a myriad of pathways and serves to replenish cellular ATP levels through down-regulation of anabolic pathways and up-regulation of catabolic pathways (Corton et al., 1994; Ferrer et al., 1985; Hardie, 2011a; Hardie et al., 2003; Yeh et al., 1980). AMPK activation has been demonstrated to inhibit the proliferation of a variety of cancer cells, resulting in activation of p53, cell-cycle arrest, and/or apoptosis depending on the cell line studied (Rattan et al., 2005; Sengupta et al., 2007; Su et al., 2007; Van Den Neste et al., 2010). While there is increasing evidence to suggest that the tumor suppressor function of AMPK is dependent on cellular and genetic context (Liang and Mills, 2013), AMPK activation holds much potential for the treatment of several other diseases including metabolic disorders (Narkar et al., 2008; Zhang et al., 2009). The metabolite 5-aminoimidazole-4-carboxamide ribonucleotide (also known as ZMP) is an allosteric activator of AMPK that is administered to cells as its permeable ribonucleoside analog, AICAR (Corton et al., 1995). It should be noted that there is discrepancy in the use of "AICAR" as an acronym in the literature; cell biologists tend to refer to the ribonucleotide as ZMP and the ribonucleoside as AICAR, whereas biochemists and chemists refer to the ribonucleotide as AICAR. To avoid potential confusion when referring to AICAR, we use the acronym adopted by cell biologists throughout. The AMPK-activating property of AICAR (via elevation of cellular ZMP) has been used to demonstrate the therapeutic potential for a molecular activator of AMPK, but the short half-life of intravenously administered AICAR, and the resulting rise in levels of blood lactic acid and uric acid, make it unsuitable for direct use as a therapeutic agent (Goodyear, 2008; Karagounis and Hawley, 2009). ZMP is also a cellular metabolite, produced in histidine biosynthesis and de novo purine biosynthesis, but ZMP is only utilized in cells by aminoimidazole carboxamide ribonucleotide transformylase/inosine monophosphate cyclohydrolase (ATIC), a bifunctional 64-kDa enzyme that catalyzes the last two steps of de novo purine biosynthesis (Ni et al., 1991). AMPK activation by exogenous ZMP (administered as the cell-permeable riboside AICAR) suggests a similar function for the endogenous metabolite, indicating the possibility of regulatory crosstalk (via ZMP) between the de novo purine biosynthesis, histidine biosynthesis, and AMPK pathways (Rebora et al., 2005; Corton et al., 1994; Xiao et al., 2007, 2011).

Homodimerization of ATIC is essential for its aminoimidazole carboxamide ribonucleotide transformylase (AICART) activity (please note that this enzyme acts on the ribonucleotide ZMP, not the corresponding ribonucleoside AICAR), as the active site of this enzyme is formed at the interface of two interacting ATIC monomers, with each molecule contributing residues (Greasley et al., 2001). An alternative approach to AMPK activation may therefore be envisaged, whereby an inhibitor of ATIC homodimerization up-regulates intracellular levels of ZMP via a metabolic block on the ninth step of the de novo purine biosynthesis pathway. The selective targeting of AICART with competitive

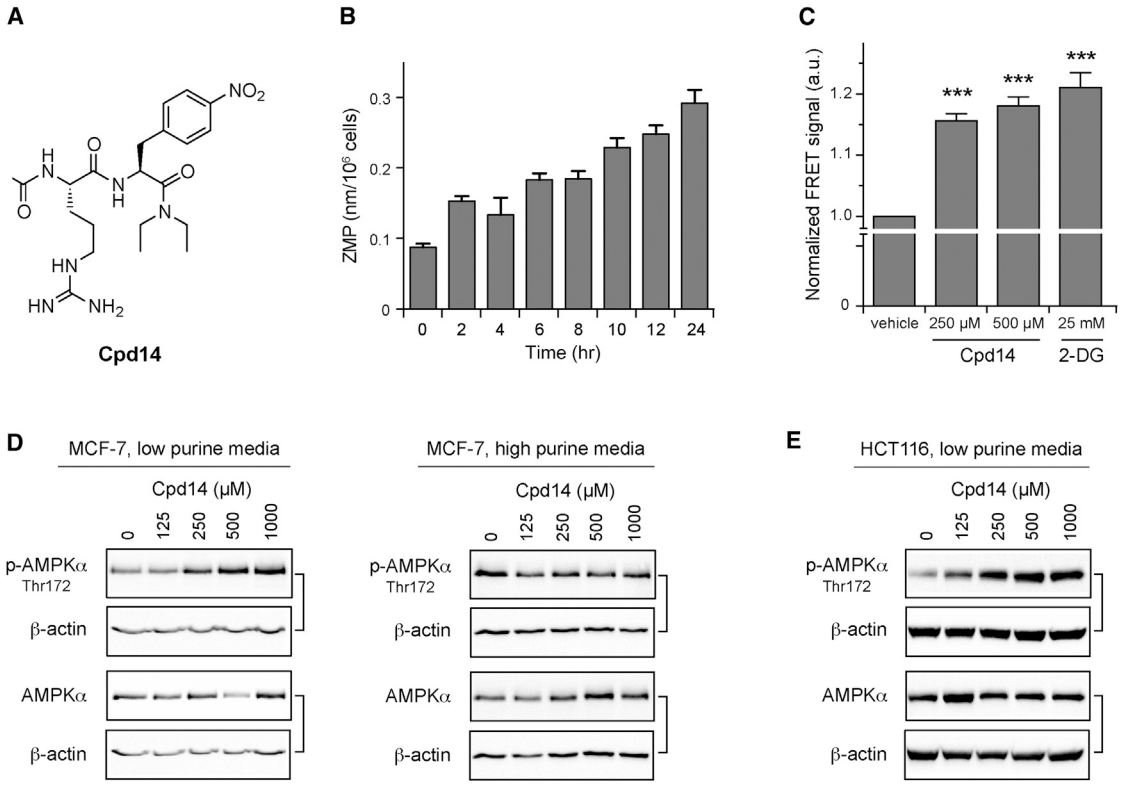

Figure 1. Cpd14 Activates AMPK in Cells by Increasing Intracellular AICAR Levels

(A) The chemical structure of Cpd14.

(B) MCF-7 cells treated with 250 μM Cpd14 show a time-dependent increase in ZMP levels.

(C) Analysis with a FRET-based AMPK activity sensor shows a 1.15- and 1.18-fold increase in AMPK activity of MCF-7 cells treated with 250 and 500 μM Cpd14, respectively. The maximum FRET signal is shown by treating MCF-7 cells with the glycolysis inhibitor 2-DG. ***$p < 0.001$.

(D) (Left) MCF-7 cells cultured in low purine medium and treated with Cpd14 display a dose-dependent increase in AMPKα Thr172 phosphorylation. (Right) Cpd14 has no effect on AMPKα Thr172 phosphorylation levels in MCF-7 cells cultured in high purine medium.

(E) HCT116 cells cultured in low purine medium treated with Cpd14 show a dose-dependent increase in AMPKα Thr172 phosphorylation. Data are mean ± SEM from three independent experiments.

substrate and cofactor analogs has proved challenging due to the widespread use of folates by cellular enzymes. Several antifolates that non-specifically inhibit ATIC have been reported (Desharnais et al., 2003; Marsilje et al., 2002, 2003), and antifolate drugs, including methotrexate, are known to also inhibit ATIC as a secondary target (Allegra et al., 1985, 1987). Recently it has been demonstrated that inhibition of AICART and a subsequent rise in intracellular ZMP plays a significant role in the antitumorigenic effects of the drug pemetrexed, which is used against non-small cell lung cancer (Racanelli et al., 2009; Rothbart et al., 2010). The dimerization requisite for AICART activity provides a mechanism by which ATIC may be selectively targeted by a protein-protein interaction inhibitor over other folate-dependent enzymes, allowing the activation of AMPK via ATIC inhibition to be further probed and examined with a specific inhibitor, and form the starting point for the development of new therapeutics. We recently reported a small-molecule inhibitor of ATIC dimerization (Spurr et al., 2012) that was developed from a cyclic hexapeptide identified using a genetically encoded high-throughput screening platform (Tavassoli and Benkovic, 2005). The molecule, named compound 14 (Cpd14, Figure 1A) was shown to inhibit AICART by disrupting ATIC homodimerization. Here, we demonstrate that inhibition of ATIC dimerization in mammalian cells with this molecule leads to up-regulation of intracellular ZMP, which in turn leads to the activation of AMPK. The in vivo effect of AMPK activation by this approach is probed using an obese mouse model, in which our compound reduces elevated blood glucose levels, improves glucose tolerance, and reduces body mass.

RESULTS

Inhibition of ATIC Homodimerization with Cpd14 Up-regulates Intracellular ZMP, and Leads to AMPK Activation

We began by measuring changes in the intracellular ZMP levels in MCF-7 cells treated with 250 μM Cpd14; the dose was chosen based on our previously reported effects of this compound on the viability of MCF-7 cells (Spurr et al., 2012). A ~1.5-fold rise in ZMP levels was observed within 2 hr of treatment, which had risen to ~3-fold after 24 hr (Figure 1B). We next probed the effect of this rise in ZMP levels on AMPK activation by two independent methods. We first used the AMPK activity reporter (AMPKAR), a fluorescence resonance energy transfer (FRET)-based biosensor of AMPK activity (Tsou et al., 2011) that directly

probes AMPK activation; we observed a 1.15-fold increase in the FRET signal in MCF-7 cells treated with 250 μM of Cpd14, which increased to 1.18-fold with 500 μM of Cpd14 (Figure 1C). We used 2-deoxyglucose (2-DG), a glucose analog that inhibits glycolysis and induces AMPK, as a positive control, and a 1.21-fold increase in the FRET signal was observed in cells treated with 25 mM 2-DG (Figure 1C). The observed values were in line with those previously reported for measuring AMPK activation with this biosensor (Tsou et al., 2011) and show that Cpd14 is activating AMPK. To further confirm activation of AMPK, we studied the effect of Cpd14 on the phosphorylation of AMPKα THR172, the major regulatory event of AMPK activation (Hawley et al., 1996; Mitchelhill et al., 1997). MCF-7 cells were treated with 125 μM, 250 μM, 500 μM, and 1 mM Cpd14, and the levels of phosphorylated and unphosphorylated AMPKα THR172 determined by immunoblot analysis. A dose-dependent increase in phosphorylation of AMPKα THR172 was observed in cells treated with Cpd14 (Figure 1D, left), further demonstrating AMPK activation by this molecule.

There are two cellular pathways for purine metabolism, the de novo purine biosynthesis pathway and the salvage pathway. In the presence of high purine levels, de novo purine biosynthesis is inhibited (Henderson and Khoo, 1965) and the salvage pathway activated (Murray, 1971); if the mechanism of action of Cpd14 is on target and as predicted, Cpd14 should be inactive under conditions where the salvage pathway is activated (as inhibition of ATIC dimerization by Cpd14 will not lead to changes to ZMP levels, thus eliminating its AMPK-activating property). We therefore assessed the AMPK-activating effects of Cpd14 in MCF-7 cells cultured in high purine cell culture medium. In line with its proposed mechanism of action, Cpd14 did not affect the phosphorylation status of AMPKα THR172 at doses up to 1 mM in MCF-7 cells cultured in high purine medium (Figure 1D, right). Cpd14 also did not affect AMPK activity in cells cultured in high glucose medium, which inactivates AMPK (Figures S1A and S1B). We next assessed the effect of Cpd14 on the phosphorylation of AMPKα THR172 in endoderm-derived HCT116 colon carcinoma cells, chosen as they are from a distinct lineage to the ectoderm/mesoderm-derived MCF-7 mammary gland adenocarcinoma cells. As with MCF-7 cells, we observed a dose-dependent increase in phosphorylation of AMPKα THR172 in cells treated with Cpd14 (Figure 1E). Together, these results demonstrate that Cpd14 places a metabolic block on the ninth step of de novo purine biosynthesis by inhibiting ATIC homodimerization, leading to increased intracellular ZMP levels and AMPK activation.

Cpd14 Regulates Downstream Targets of AMPK and Cell Viability

The effect of Cpd14 on AMPK signaling was further probed by examining downstream AMPK targets. We first assessed the phosphorylation state of Ser79 of acetyl-CoA carboxylase (ACC), a direct target of activated AMPK (Munday et al., 1988), which is inactivated by phosphorylation and frequently used as an indicator of AMPK activity in cells (Winder and Hardie, 1996). We observed a dose-dependent increase in ACC Ser79 phosphorylation in MCF-7 cells treated with Cpd14 (Figure 2A). A similar effect from Cpd14 was observed in HCT116 cells, with a dose-dependent increase in ACC Ser79 phosphorylation observed in cells treated with Cpd14 (Figure 2B). Given that ACC phosphorylation is a sensitive measure of AMPK activity, we monitored the effect of 250 μM Cpd14 on ACC Ser79 phosphorylation in MCF-7 cells over time. An increase in ACC Ser79 phosphorylation was visible within 2 hr of CMP14 administration (Figure 2C), with a time-dependent increase in the intensity of the band associated with this protein (Figure 2C). We again assessed the on-target nature of the observed effect from Cpd14 using high purine cell culture medium. As observed for AMPK phosphorylation, Cpd14 had no effect on ACC phosphorylation under these conditions (Figure S2), indicating that the observed effects are a result of the metabolic block placed on step 9 of de novo purine biosynthesis and the subsequent rise in intracellular ZMP.

The phosphorylation state of Ser240 and Ser244 of p70 ribosomal protein S6 (S6) and the phosphorylation state of Thr56 of eukaryotic elongation factor 2 (eEF2) are other commonly used markers of AMPK activity (Rothbart et al., 2010; Vainer et al., 2014). S6 is regulated by AMPK through the mTOR (mammalian target of rapamycin) complex; activation of AMPK represses mTOR activity, leading to a reduction in S6 kinase 1 activity, which in turn reduces phosphorylation of S6. An AMPK activator would therefore be expected to cause a reduction in phosphorylation of S6. In MCF-7 cells, we observed a dose-dependent reduction in S6 phosphorylation upon treatment with Cpd14 (Figure 2D). A similar reduction in S6 phosphorylation was also observed in HCT116 cells upon treatment with Cpd14 (Figure 2E). Activated AMPK directly targets eEF2 kinase, leading to hyperphosphorylation of eEF2; a dose-dependent increase in eEF2 phosphorylation was observed upon treatment of MCF-7 cells with Cpd14 (Figure 2F), in line with the AMPK-activating property of Cpd14.

We next assessed the effect of Cpd14 on the proliferation and viability of MCF-7 and HCT116 cells. As expected from an AMPK activator, a dose-dependent reduction in cell numbers was observed in both HCT116 and MCF-7 cells treated with Cpd14, with a significant effect observed at 250 μM and higher doses (Figure 3A). Interestingly, HCT116 cells did not show a further significant decrease in cell numbers at doses higher than 250 μM, while a dose-dependent decline in cell number was observed in MCF-7 cells, with ~40% reduction in cell numbers following treatment with 1 mM Cpd14. The effect of Cpd14 on cell proliferation and viability was further probed via 3-(4,5-dimethylthiazol-2-yl)-2,5-diphenyltetrazolium bromide (MTT) assay, and a dose-dependent reduction in cell growth was again observed in both cell lines (Figure 3B). The ratio of the number of live cells versus total particles (arising from cell death and apoptosis) was next assessed using a microfluidic-based cell counter. Cpd14 at doses up to 1 mM did not cause a significant effect on the ratio of live to dead cells (Figure 3C), indicating that the observed reduction in proliferation with Cpd14 is due to cytostatic rather than cytotoxic effects. We next assessed the effect of Cpd14 on the clonogenicity of MCF-7 cells (Figure 3D), and observed a dose-dependent reduction in colony numbers (Figure 3E). Together, these data demonstrate that the effect of Cpd14 on cell proliferation and viability is due to a reduction in cell division, which is consistent with AMPK activation by Cpd14.

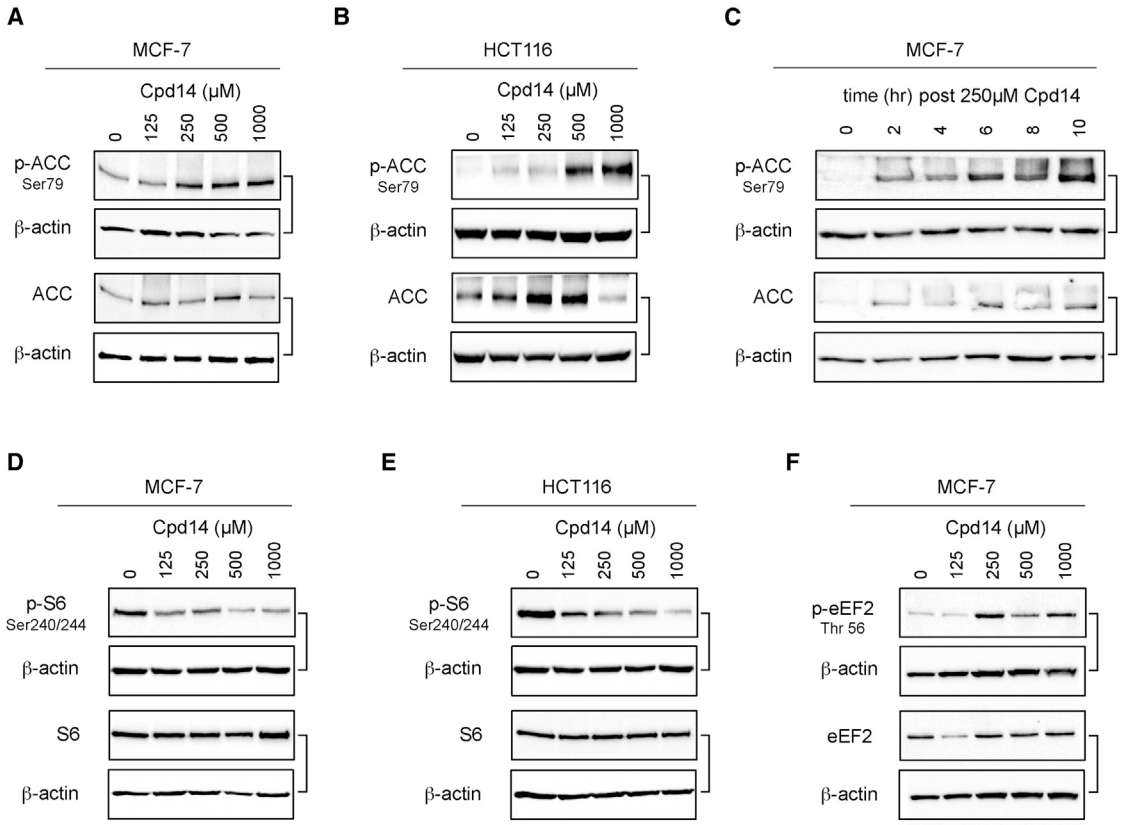

Figure 2. Cpd14 Activates AMPK Signaling in Cells

(A) MCF-7 cells treated with Cpd14 show a dose-dependent increase in ACC Ser79 phosphorylation.
(B) HCT116 cells treated with Cpd14 show a dose-dependent increase in ACC Ser79 phosphorylation.
(C) MCF-7 cells treated with 250 μM Cpd14 show a time-dependent increase in ACC Ser79 phosphorylation.
(D) MCF-7 cells treated with Cpd14 cells show a dose-dependent decrease in S6 Ser240/244 phosphorylation.
(E) HCT116 cells treated with Cpd14 show a dose-dependent decrease in S6 Ser240/244 phosphorylation.
(F) MCF-7 cells treated with Cpd14 show a dose-dependent increase in eEF2 Thr56 phosphorylation.

Activation of AMPK by Cpd14 Increases Cellular Oxygen Uptake and Reduces Lactate Levels

A key effect of AMPK activation is on cell metabolism; selective activation of AMPK has been proposed as a potential therapeutic for diabetes and metabolic syndrome (Hardie, 2011a, 2011b; Viollet et al., 2006; Zhang et al., 2009). We therefore probed the effect of Cpd14 on the metabolism of MCF-7 cells by measuring changes in oxygen consumption and lactic acid levels upon treatment with Cpd14. We observed a 1.4-fold increase in mean oxygen consumption upon treatment with 250 μM Cpd14, from 16.3 ± 0.7 to 22.5 ± 0.6 μl O_2/mg protein/hr (Figure 3F). For comparison, treatment with 500 μM AICAR led to a 1.2-fold increase in oxygen consumption to 20 ± 0.8 μl O_2/mg protein/hr (Figure 3F). We next measured the effect of Cpd14 on lactic acid accumulation in the culture medium of MCF-7 cells. We observed a 1.25-fold decrease in lactate levels, from 17.4 ± 1.1 to 13.8 ± 1.1 nl lactate/mg protein/hr in the culture medium of cells treated with 250 μM Cpd14, and a dose-dependent 1.44-fold decrease in lactate (to 12.3 ± 1.1 nl lactate/mg protein/hr) for cells treated with 500 μM Cpd14 (Figure 3G). For comparison, a 1.3-fold decrease in lactate was observed in the culture medium of cells dosed with 500 μM AICAR (to 13.4 ± 0.7 nl lactate/mg protein/hr), while baseline lactate was measured as 9.3 ± 0.3 nl lactate/mg protein/hr (1.9-fold reduction) for cells treated with 20 mM 2-DG (Figure 3G). The increase in intracellular oxygen consumption and decrease in extracellular levels of lactic acid observed in response to treatment with Cpd14 are in line with its function as an AMPK activator.

Cpd14 Treatment Reduces Blood Glucose Levels, Improves Glucose Tolerance, and Reduces Body Mass in an Obese Mouse Model

Previous studies have shown that AMPK activation in the liver controls glucose homeostasis through (direct and indirect) inhibition of gluconeogenesis, while AMPK activation in muscle tissue mediates the beneficial effects of exercise, such as increased fatty acid oxidation (Fullerton et al., 2013; Viollet et al., 2006, 2009, 2010; Zhang et al., 2009). In addition, AMPK activation by AICAR has been demonstrated to act as an exercise mimetic in sedentary mice (Narkar et al., 2008). We therefore sought to assess the effect of Cpd14 on blood glucose and body mass in vivo; however, we first assessed the pharmacokinetic properties of the molecule. Cpd14 was found to have excellent stability in mouse and human microsomes, with a half-life of more than 3 hr in each. Cpd14 was also stable in human plasma,

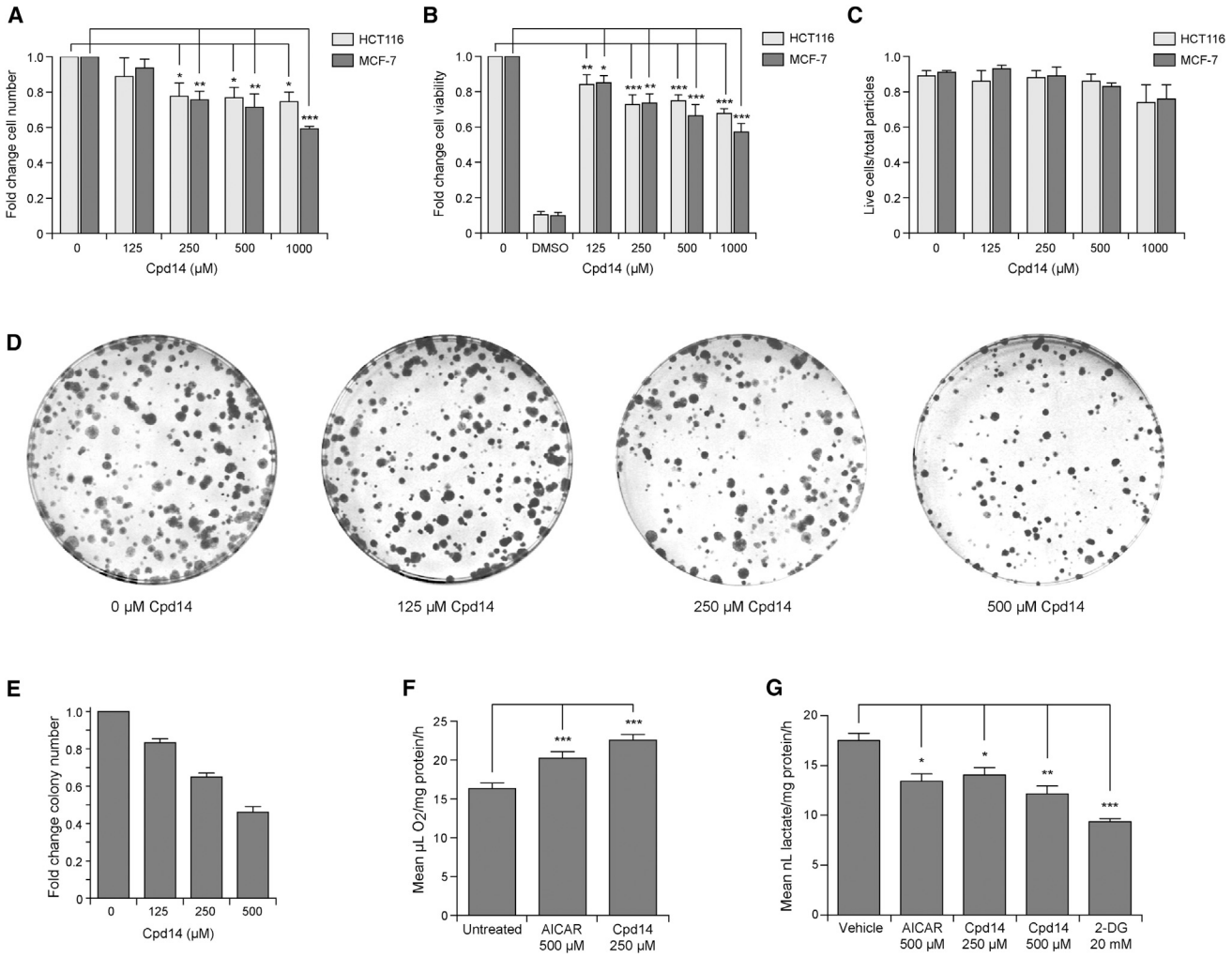

Figure 3. Cpd14 Reduces Viability, Increases Oxygen Usage, and Reduces Lactate Levels in Cells

(A) Effect of Cpd14 on cell number in MCF-7 and HCT116 cells 48 hr after treatment (n = 3, each count in duplicate).

(B) Effect of Cpd14 on cell viability in MCF-7 and HCT116 cells, measured by MTT assay 48 hr after treatment. 3% DMSO was used as a control (n = 3, each in triplicate).

(C) Effect of Cpd14 on the ratio of living cells versus total particles in MCF-7 and HCT116 cells (n = 3, each in duplicate).

(D) Treatment with Cpd14 affects clonogenic survival of MCF-7 cells.

(E) Quantification of clonogenic assay (n = 3).

(F) Oxygen consumption of MCF-7 cells 24 hr after treatment with 500 μM AICAR or 250 μM Cpd14 (n = 5, each in triplicate).

(G) Production of lactic acid in MCF-7 cells treated with 500 μM AICAR, 250 μM Cpd14, 500 μM Cpd14, or 2 mM of the glycolysis inhibitor 2-DG (n = 3, each in triplicate).

Data shown are mean ± SEM from three independent experiments. For all data, *p < 0.05, **p < 0.01, ***p < 0.001.

with no degradation observed after 2 hr of exposure. The kinetic solubility of the molecule was also good at 201 μM. The LogD for the molecule was relatively low at −0.7, and, likely as a result of this, the permeability of the molecule (measured by PAMPA) was also low, at 1 nm/s. These data suggest that poor cell permeability may be the source of the disparity between the activity of Cpd14 in vitro (K_i of 685 nM) and its active dose in cells (250 μM).

We next examined the effect of Cpd14 in vivo; glucose tolerance and body mass was measured in 15-week-old male C57BL/6 mice fed either the standard chow diet (7% kcal fat) or a high-fat diet (45% kcal fat). The high-fat diet resulted in heavier and fatter animals, which are glucose intolerant and have elevated fasting blood glucose levels (Bruce et al., 2009). We began by measuring the effect of a single dose of Cpd14 (intraperitoneally [i.p.], 0.05 mg/g body weight) or vehicle (saline) on the blood glucose level of animals that were fasted overnight. In the chow-fed group, the blood glucose level of the vehicle-treated mice remained unchanged within error (from 6.44 ± 0.1 to 6.70 ± 0.2 mmol/l) after 3 hr, while the Cpd14-treated group showed a 21% reduction in blood glucose (from 6.47 ± 0.2 to 5.13 ± 0.2 mmol/l) after 3 hr (Figure 4A). The blood glucose level of the high-fat-fed group was significantly elevated compared with that in chow-fed mice. Treating the high-fat-fed

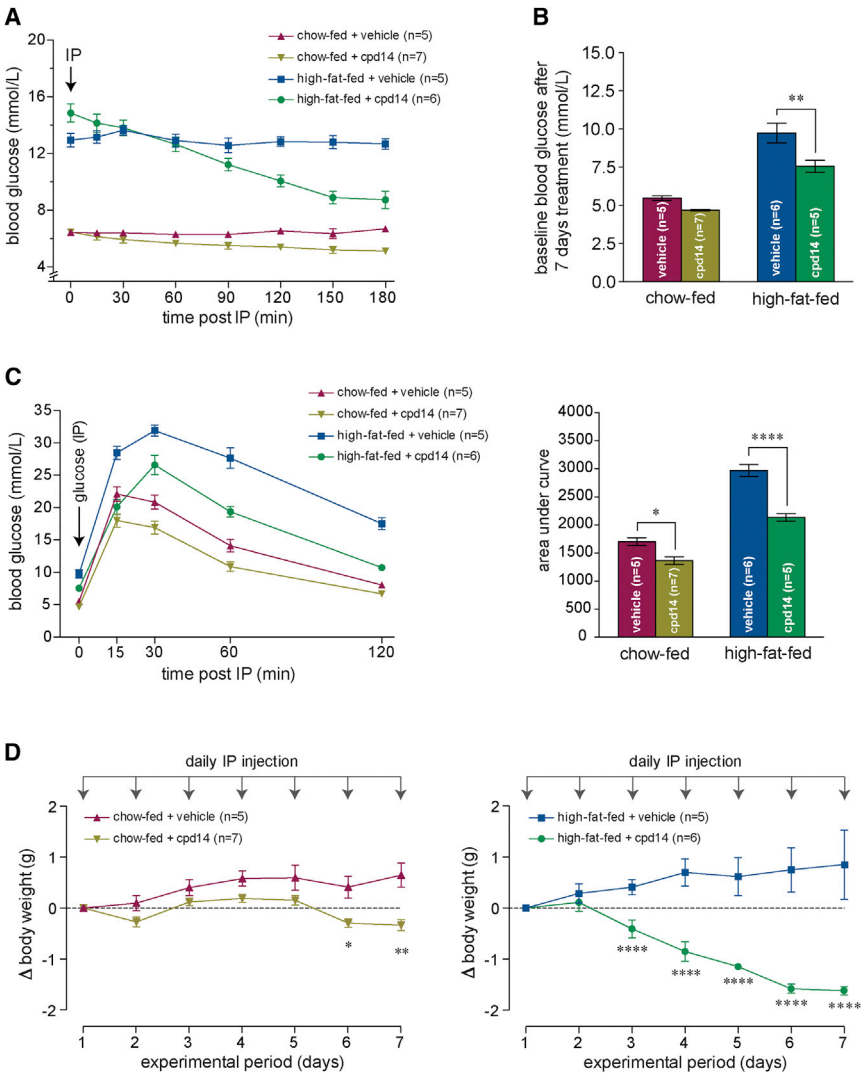

Figure 4. The Effect of Cpd14 on Glucose Metabolism in C57BL/6 Mice

(A) 3-hr blood glucose levels after administration of Cpd14 or vehicle (intraperitoneally [i.p.] at 0.05 mg/g) in chow-fed or high-fat-fed 15-week-old C57BL/6 male mice.

(B) Baseline blood glucose level after 7 days of Cpd14 or vehicle administration (i.p. at 0.05 mg/g) in 15-week-old C57BL/6 male mice.

(C) (Left) Blood glucose level during 2-hr glucose tolerance test after 7 days of Cpd14 or vehicle administration (i.p. at 0.05 mg/g) in chow-fed or high-fat-fed 15-week-old C57BL/6 male mice. (Right) Area under the curve for the graph on the left.

(D) Change in body mass over 7 days of Cpd14 or vehicle administration (i.p. at 0.05 mg/g) in (left) chow-fed 15-week-old C57BL/6 male mice and (right) high-fat-fed 15-week-old C57BL/6 male mice. Average body mass of chow-fed mice = 29.1 ± 0.2 g; average body mass of high-fat-fed mice = 35.8 ± 2.4 g.

All data shown are mean ± SEM. For all data, *p < 0.05, **p < 0.01, ****p < 0.0001.

mice with vehicle did not significantly change the blood glucose level over 3 hr (from 12.9 ± 0.5 to 12.6 ± 0.4 mmol/l), whereas those treated with Cpd14 showed a 42% drop in blood glucose levels (from 14.87 ± 0.6 to 8.74 ± 0.6 mmol/l) after 3 hr (Figure 4A).

We next probed the effect of repeated Cpd14 treatment on baseline glucose levels and glucose handling. Mice in the chow-fed and high-fat-fed group were given a single dose of Cpd14 or vehicle per day, for 7 days; after this time, the baseline fasting glucose level of each group was measured. It should be noted that the high-fat-fed mice were kept on this diet throughout these 7 days. Cpd14 had an insignificant effect on fasting blood glucose levels in the chow-fed group; vehicle-treated mice had a fasting blood glucose level of 5.50 ± 0.14 mmol/l, compared with 4.71 ± 0.06 mmol/l for those treated with Cpd14 (Figure 4B). In contrast, seven daily doses of Cpd14 had significantly reduced fasting blood glucose in the high-fat-fed group; vehicle-treated animals had a glucose level of 9.76 ± 0.64 mmol/l, compared with 7.58 ± 0.40 mmol/l for the Cpd14-treated animals (Figure 4B). We next examined glucose handling in these animals (treated with 7× daily doses of vehicle or Cpd14) using a glucose tolerance test. Each group was injected with D-glucose (2 mg/g body weight), and their blood glucose level monitored for the following 2 hr. Cpd14 had improved glucose clearance in the chow-fed group, with a blood glucose level after 2 hr of 8.06 ± 0.36 mmol/l for the vehicle-treated group versus 6.68 ± 0.44 mmol/l in the Cpd14-treated animals (Figure 4C, left). Cpd14 treatment resulted in a 20% reduction in the area under curve in the chow-fed group (Figure 4C, right). In the high-fat-fed group, there was a much greater rise in blood glucose levels following glucose administration, and poor glucose clearance, indicating impaired glucose tolerance. As before, the effects of Cpd14 were amplified in this high-fat-fed group; we observed significantly improved glucose clearance in the Cpd14-treated, high-fat-fed group (Figure 4C, left), with ~40% difference in blood glucose level after 2 hr between the vehicle-treated (17.51 ± 0.89 mmol/l) and Cpd14-treated group (10.76 ± 0.43 mmol/l). This corresponded to ~30% reduction in the area under curve for the Cpd14-treated group (Figure 4C, right).

We also assessed the effect of Cpd14 on the body mass of the aforementioned animals treated with 7× daily doses of vehicle or Cpd14. The average weight of the chow-fed group (initial weight of 29.1 ± 0.2 g) had increased by 0.64 ± 0.53 g in vehicle-treated animals, while it had decreased by 0.37 ± 0.28 g in the Cpd14-treated group (Figure 4D, left). In contrast to this minor change, the average weight of the high-fat-fed group (initial weight of 35.8 ± 2.4 g) was significantly reduced in the Cpd14-treated animals; those treated with vehicle showed a 0.85 ± 0.67 g increase in body mass, whereas a daily dose of Cpd14 for 7 days had resulted

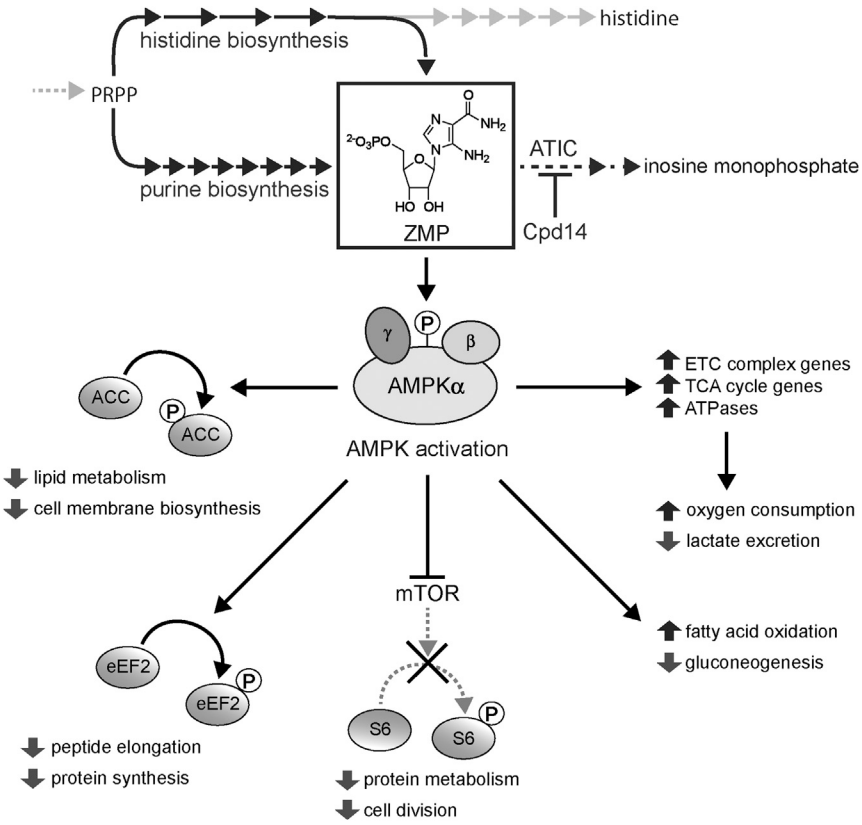

Figure 5. AMPK Activation by Cpd14

Inhibition of ATIC homodimerization by Cpd14 leads to an increase in endogenous ZMP, which activates AMPK and its downstream pathways. ETC, electron transport chain; mTOR, mammalian target of rapamycin; PRPP, phosphoribosyl pyrophosphate; TCA, tricarboxylic acid.

in a 1.62 ± 0.83 g reduction in body mass per animal, despite continued consumption of the high-fat diet (Figure 4D, right).

DISCUSSION

Exogenously administered ZMP (as the cell-permeable ribonucleoside AICAR) has long been known to function as an allosteric activator of AMPK (Corton et al., 1995), serving as a valuable research tool to allow significant insight into regulation of cellular energetics (Hardie, 2011b). Here, we demonstrate that endogenous ZMP is also capable of activating AMPK by placing a metabolic block on the ninth step of de novo purine biosynthesis using an inhibitor of ATIC homodimerization (Figure 5). ZMP is synthesized in cells by two independent pathways (histidine biosynthesis and de novo purine biosynthesis), but only utilized in purine biosynthesis; previous work in yeast has demonstrated that ZMP is more than just a metabolite, with significant crosstalk between these two pathways occurring through ZMP (Rebora et al., 2005). Unlike mammalian cells, however, the yeast analog of AMPK (SNF1) is activated by ADP rather than AMP (Mayer et al., 2011), hence ZMP does not regulate SNF1 activity in yeast (Pinson et al., 2009). The AMPK-activating property of ZMP in mammalian cells is unlikely to be coincidental; this regulatory molecule (ZMP) potentially links histidine and de novo purine biosynthesis to AMPK signaling in cells. Further studies are required to fully decipher this regulatory role of endogenous ZMP in mammalian cells.

Here, we have used the perquisite of ATIC dimerization for AICART activity to probe the effect of endogenous ZMP on AMPK activation, but it should be noted that any inhibitor of AICART should also share the AMPK-activating property of Cpd14. AICART uses 10-formyltetrahydrofolate as a substrate, and as a result is targeted by many antifolates; for example, a previous study suggests that the principal mode of metabolic inhibition by methotrexate in MCF-7 cells is via inhibition of AICART activity (Allegra et al., 1987). In line with our observations, Allegra et al. (1987) measured a 2- to 3-fold increase in the intracellular ZMP pool, but as this work was conducted prior to the discovery of AMPK (Carling et al., 1989), the implications of this rise in endogenous ZMP levels for AMPK activity could not be explored. More recent work with pemetrexed, an antifolate used in the treatment of non-small cell lung carcinoma, has further probed this possibility (Racanelli et al., 2009). The primary targets of pemetrexed are dihydrofolate reductase, thymidylate synthase, and GAR Tfase (Shih et al., 1997), with AICART being a secondary target. Using a series of elegant experiments, Moran and co-workers have demonstrated the AMPK-activating property of pemetrexed, and have determined that this effect, mediated through a rise in endogenous ZMP arising from AICART inhibition, is a key component of the anticancer properties of pemetrexed (Racanelli et al., 2009; Rothbart et al., 2010). Cpd14 lacks the folate backbone of the aforementioned molecules, instead targeting AICART activity by inhibiting homodimerization and the formation of the active quaternary structure (Spurr et al., 2012; Tavassoli and Benkovic, 2005). Given its unique mode of action and resulting specificity, Cpd14 provides the possibility of directly probing the role of ZMP and ATIC in cells.

In addition to the effects of Cpd14 on AMPK and mTOR signaling, we also observed increased cellular oxygen consumption and decreased lactic acid production. Activated AMPK can directly phosphorylate enzymes that cause the up-regulation of oxidative phosphorylation and increases in oxygen consumption (Jager et al., 2007; Narkar et al., 2008). However, it has been shown that putative activators of AMPK do not necessarily lead to up-regulated oxidative phosphorylation. Treatment with metformin, for example, which has previously been shown to activate AMPK in cells (Hawley et al., 2002; Shaw et al., 2005), opposes stimulation of oxidative phosphorylation. In contrast, treatment with AICAR augments this pathway (Cheong et al., 2011); our data show that Cpd14 acts in the same way as AICAR, in line with its proposed mechanism of action (Figure 5).

In our in vivo studies, Cpd14 treatment was found to reduce blood glucose levels and improve glucose tolerance. This effect of Cpd14 was significantly more prominent in mice that were made obese and glucose intolerant by being fed a high-fat diet. Given our observations in cells, the reduction in blood glucose following an acute dose and the improvement in glucose tolerance following chronic treatment is most likely due to activation of AMPK by Cpd14. AMPK activation is known to inhibit hepatic gluconeogenesis (Kahn et al., 2005; Ruderman et al., 2013), increase muscle glucose uptake (Steinberg and Kemp, 2009), and promote glucose metabolism by increasing mitochondrial biogenesis (Steinberg and Kemp, 2009). Further studies are needed to ascertain the mechanisms by which Cpd14 controls glucose homeostasis in vivo, but one possible route may be via the increased phosphorylation of ACC by Cpd14 observed in our cell assays. This reduces ACC activity, which is a requisite for the maintenance of glucose homeostasis (O'Neill et al., 2014). We likewise found a marked reduction in body weights of the obese mice following chronic (7 days) treatment with Cpd14; these mice appeared normal throughout our study, so the reduction in weight was not due to any malaise or change in behavior. While an effect from Cpd14 on the appetite of these animals cannot be ruled out, the lack of weight loss in the Cpd14-treated chow-fed mice suggests that this is not the case; similar effects have only previously been observed when there is marked improvement in glucose homeostasis and enhanced fat oxidation (Goodpaster et al., 2003). Activation of AMPK is known to increase the expression of uncoupling protein 1 in adipose tissue and thermogenesis (Vila-Bedmar et al., 2010), and it will interesting to determine in future studies whether there is a reduction in adipose depots in the high-fat-fed obese mice treated with Cpd14. Our current results suggest that there is much potential for Cpd14 as a treatment for diabetes as, unlike current antidiabetic drugs, this compound could improve glucose handling as well as reduce the body weight of obese diabetic patients.

SIGNIFICANCE

AMPK is the central sensor of cellular energy homeostasis, whose selective activation has been a long-standing goal in drug discovery; activation of AMPK is proposed to be of therapeutic benefit in several disorders including cancer and metabolic syndrome. A widely used allosteric activator of AMPK is AICAR, a cell-permeable nucleoside that is converted to the active nucleotide (ZMP) in cells. AICAR is administered to cells at 1–5 mM levels and widely used in the laboratory. ZMP is also a metabolite, produced by de novo purine biosynthesis and histidine biosynthesis, but only used by a homodimeric, bifunctional enzyme called ATIC that catalyzes the final two steps of de novo purine biosynthesis. We use our selective inhibitor of ATIC homodimerization to place a metabolic block on the ninth step of purine biosynthesis, which leads to an increase in intracellular ZMP. We demonstrate that this increase in endogenous ZMP activates AMPK and its downstream signaling pathways. We go on to demonstrate the possibility of using this approach as a therapeutic strategy with a mouse model for metabolic syndrome. Our results not only demonstrate a new molecular approach to selective AMPK activation, but also suggest that AICAR acts as a regulatory molecule that links two biosynthetic pathways to AMPK activity.

EXPERIMENTAL PROCEDURES

All reagents were purchased from Fisher Scientific unless otherwise stated. 2-DG and ZMP were purchased from Sigma. Cpd14 was synthesized as previously detailed (Spurr et al., 2012). Statistical analysis was performed using GraphPad Prism and MiniTab 16. All values are expressed as the mean ± SEM. Values of $p < 0.05$ were considered statistically significant. Western blots shown are representative images from triplicates.

Cell Culture, Cell Treatments, Transfection, and Cell Counting

All cell culture reagents were purchased from Life Technologies unless otherwise stated. Cell lines were sourced from the American Type Culture Collection and not grown continually for more than 3 months. All cells were cultured at 37°C in a humidified 5% CO_2 atmosphere. MCF-7 cells were routinely maintained in DMEM containing 10% fetal bovine serum (FBS) and 1% penicillin/streptomycin, and HCT116 cells in McCoy's 5A medium supplemented with 10% FBS and 1% penicillin/streptomycin. Unless otherwise stated, cells were dosed with 250 μM Cpd14 in reduced glucose medium (10 mM or 15 mM glucose for MCF-7 and HCT116 cells, respectively), supplemented with 10% purine-free dialyzed FBS, in 0.5% (v/v) DMSO. Cells were passaged in reduced glucose medium prior to experiments. Transient transfection was carried out using FuGENE HD (Promega) according to the manufacturer's instructions, and experiments were carried out 24 hr after transfection. Cell counts and live/dead cell ratios were obtained using a Moxi Z Mini automated cell counter (Orflo).

HPLC Nucleotide Analysis

MCF-7 cells were dosed with Cpd14 as described above and harvested at different time points. Cells were detached using warm 0.05% (w/v) trypsin/EDTA solution, washed in PBS, and the resulting cell pellet resuspended in ice-cold 5% (w/v) trichloroacetic acid at a density of approximately 10^6 cells per 200 μl trichloroacetic acid. Cells were then briefly vortexed, held on ice for 5 min, and debris removed by centrifugation at 2,500 rpm for 5 min. The acid-soluble fraction was neutralized by three extractions with diethyl ether, and the lower fraction containing the nucleotides kept between each extraction. Concurrent nucleotide extractions were then pooled and lyophilized. For high-performance liquid chromatography (HPLC) analyses, samples were passed through a 0.22-μM syringe filter prior to injection into a SUPELCOSIL LC-18-T 250 × 4.6-mm reverse-phase HPLC column (Sigma). Samples were eluted at a flow rate of 0.8 ml/min using the following ratios for each elution buffer: 0.1 M KH_2PO_4 (pH 6) and 90% methanol, (1:0) first 0–15 min; (4:1) 15–17.5 min; (1:9) 17.5–23 min; (0:1) 24–34 min. Absorbance was monitored at 254 nm. Nucleotides were detected using their absorbance at 254 nm and compared with the elution position of standard solutions of ATP, ADP, AMP, ZMP, and NAD^+ (all from Sigma). The area under the peaks was quantified by integration using Empower Pro software (Waters) and ZMP concentration determined by fitting peak absorbance to a standard curve generated from synthetic nucleotides. It should be noted that AMPK activation has been observed in cells detached with trypsin (Page and Lange, 1997), and although there is no evidence that this alters the intracellular ZMP levels, the values quoted for intracellular ZMP levels may not directly reflect ZMP levels prior to detachment.

AMPK Activity Fluorescence Reporter Assay

The plasmid encoding AMPKAR was used as previously described (Tsou et al., 2011). In brief, MCF-7 cells were seeded at 7,000 cells per well in black 96-well plates 16 hr prior to transfection of the AMPKAR construct using FuGENE HD (Promega), followed by incubation at 37°C for 24 hr. Cells expressing AMPKAR were then dosed with Cpd14 or 2-DG for 48 hr, followed by gentle washing and resuspension in PBS prior to independently measuring the fluorescence of the donor eCFP fluorophore (C; excitation 439 nm/emission 476 nm) and acceptor Venus-YFP fluorophore (Y; excitation 515 nm/emission 528 nm) on

a microplate reader (Tecan Infinite M200 Pro). Analysis of the FRET signal responses to each treatment type was performed by calculating the normalized mean (Y/C) emission ratio.

Protein Immunoblotting

Cells were washed with ice-cold PBS and harvested on ice. Cells were lysed by incubation on ice for 15 min with radioimmunoprecipitation assay (RIPA) buffer (50 mM Tris [pH 7.4], 150 mM NaCl, 10% [v/v] sodium-deoxycholate, 10% [v/v] IGEPAL CA-630; Sigma) containing protease inhibitor cocktail and PhosSTOP (Roche). Lysates were sonicated for 1 min in a sonicating water bath and then centrifuged at 10,500 rpm for 10 min at 4°C. The protein concentration in the supernatant was quantified by the Bradford assay. The protein samples were divided in two, and separate gels were run for phosphorylated and non-phosphorylated proteins. Proteins were separated on 8%–12% SDS-polyacrylamide Bis-Tris gels under denaturing conditions, transferred to unsupported pure nitrocellulose membrane (Amersham), and subjected to immunoblot analysis.

Rabbit monoclonal primary antibodies raised against AMPKα (D5A2, 1:500), phospho-AMPKα (Thr172, 40H9, 1:500), ACC (C83B10, 1:500), phospho-acetyl-CoA carboxylase (Ser79, D7D11, 1:500), phospho-S6 ribosomal protein (Ser240/244, 1:5,000), and S6 ribosomal protein (1:5,000; Cell Signaling Technology) were used for blotting. Antibodies were diluted in Tris-buffered saline containing 5% BSA and 0.1% Tween 20, and incubated with the membrane overnight at 4°C. Horseradish peroxidase-conjugated antirabbit immunoglobulin G antibody (NA934, 1:10,000; GE Healthcare) was used as the secondary antibody, and monoclonal anti-β-actin-peroxidase antibody (A3854, 1:50,000; Sigma) served as a loading control. Bound immunocomplexes were detected using ECL prime western blot detection reagent (RPN2232; GE Healthcare) and analyzed using Image Lab 4.0 computer software (Bio-Rad).

Cell Viability Assays

MCF-7 cells and HCT116 cells were seeded in triplicate at 6,000 cells per well and 10,000 cells per well, respectively, on 96-well plates 16 hr prior to dosing with Cpd14 in 200 μl of fresh medium; final concentration of solvent DMSO in each well was 0.5% (v/v). MTT-based cell proliferation assays were performed 48 hr after dosing, as follows: MTT (Sigma) was prepared in sterile PBS and added to cells to a final concentration of 1 mM (10% v/v). Cells were then incubated for 4 hr at 37°C until intracellular punctate purple precipitates were clearly visible under the microscope. An equal volume of DMSO was then added, and the cells incubated for 10 min in the dark at room temperature with agitation to dissolve the insoluble formazan particles. Absorbance was measured at 570 nm on a microplate reader (Tecan Infinite M200 Pro).

Clonogenic Assays

MCF-7 cells were seeded at 800 cells per dish in 6-cm dishes 16 hr prior to dosing with 250 μM Cpd14 for 48 hr. Cells were then gently washed in PBS and fresh medium added, and they were incubated for up to 14 days with fresh medium added every 48–72 hr. At the end of the experiment cells were fixed by addition of methanol/acetic acid (3:1) for 5 min, then stained by incubating with 0.5% (v/v) crystal violet solution (diluted in methanol) for 10 min, and colonies counted.

Oxygen Consumption Assays

Extracellular oxygen consumption was measured using oxygen biosensor 96-well microplates (BD Biosciences) according to the manufacturer's instructions. In brief, cells pre-treated for 24 hr with test compounds were seeded in triplicate on biosensor microplates at a cell density of 1×10^6 cells/ml following equilibration of the plate at 37°C for 30 min. Deionized water and freshly prepared 100 mM Na_2SO_3 were also added to represent 20% oxygen and 0% oxygen controls, respectively. Test compounds were reintroduced to cells and the plate covered with an airtight seal. Fluorescence (485 nm excitation/620 nm emission) was measured every 2 min for approximately 1 hr using a microplate reader (BMG). At the end of the experiment cells were harvested from the plate, lysed, and total cell protein extracted using RIPA buffer as described above, and quantified by Bradford assay. Oxygen consumption over the 1-hr test period was calculated from the slope of the graph produced and standardized to the 0% and 20% oxygen controls, before being normalized to the amount of protein present in each sample.

Lactate Production Assays

Lactate in culture medium was measured with the colorimetric L-Lactate Assay Kit (Abcam) according to the manufacturer's instructions. MCF-7 cells were seeded at 400,000 cells per 25-cm^2 flask, 16 hr prior to dosing with 250 and 500 μM Cpd14, 500 μM AICAR, or 20 mM 2-DG for 24 hr. Cells were then washed in PBS and fresh medium added. Medium samples (representing less than 2% of the total volume) were then collected at different time points, filtered through a 10-kDa molecular weight cutoff centrifugal filter (Millipore) to remove all proteins, diluted 100-fold, and added at 50 μl/well to a 96-well plate, along with 50 μl/well of reaction mix. Samples were incubated at room temperature for 30 min and absorbance measured at 450 nm on a microplate reader (Tecan Infinite M200 Pro). At the end of the experiment cells were lysed and total protein extracted as described above, and quantified by Bradford assay.

In Vivo Studies

All experiments were carried out in accordance with the UK Animals (Scientific Procedures) Act 1986. Male C57/BL6J mice were used in the study and were maintained under a 12-hr light/dark cycle (lights on at 07:00), and at a constant temperature of 22°C ± 2°C with food and water available ad libitum. At 4 weeks of age the mice were randomly allocated to one of two diets: standard chow (C; 7% kcal fat, 18% kcal protein, 75% kcal carbohydrate; Special Dietary Services UK), or a high-fat diet (45% kcal fat, 20% kcal protein, 35% kcal carbohydrate; Special Dietary Services UK). In one study, mice from both dietary groups were fasted overnight at 15 weeks of age. Fasting glucose concentration was measured from whole blood obtained from the tail vein before the mice were injected i.p. with either Cpd14 (dissolved in 0.9% saline [w/v]) at a dose of 0.05 mg/g mouse body weight or the vehicle (physiological saline). Blood glucose concentration was then assayed using an Aviva Accu-Chek glucometer (Roche Diagnostics Ltd UK) at 15, 30, 60, 90, 120, 150, and 180 min post i.p. injection. In another study, 15-week-old mice were given a daily i.p. injection of Cpd14 or vehicle for 7 days. The body weights of the mice were measured daily during this period. After 7 days of treatment, mice were fasted overnight and injected i.p. with D-glucose (2 g/kg mouse body weight) for a 2-hr glucose tolerance test.

SUPPLEMENTAL INFORMATION

Supplemental Information includes two figures and can be found with this article online at http://dx.doi.org/10.1016/j.chembiol.2015.06.008. In accordance with Research Councils UK's data sharing policy, the raw data from the above experiments is available from the University of Southampton data repository.

AUTHOR CONTRIBUTIONS

A.T. conceived, designed, and supervised the project. D.J.A. conducted all cell-based experiments and assays. F.C. synthesized Cpd14. M.B. conducted the nucleotide quantification assay. F.D.H. designed and supervised the oxygen consumption assay. F.R.C. designed and conducted the in vivo experiments. A.T. wrote the manuscript with input from all authors.

ACKNOWLEDGMENTS

The authors thank Dr. Andy Merritt and Dr. Mike J. Waring for assistance with the pharmacokinetic studies, and Prof. Lewis C. Cantley for the plasmid encoding AMPKAR. We also thank the Engineering and Physical Sciences Research Council (EP/H04986X/1 to A.T.), Cancer Research UK (A10263 to A.T.), Medical Research Council (G0701153 to F.D.H.), and Diabetes UK (11/0004377 to F.R.C.) for funding this work.

Received: January 19, 2015
Revised: May 28, 2015
Accepted: June 2, 2015
Published: July 2, 2015

REFERENCES

Allegra, C.J., Drake, J.C., Jolivet, J., and Chabner, B.A. (1985). Inhibition of phosphoribosylaminoimidazolecarboxamide transformylase by methotrexate and dihydrofolic acid polyglutamates. Proc. Natl. Acad. Sci. USA *82*, 4881–4885.

Allegra, C.J., Hoang, K., Yeh, G.C., Drake, J.C., and Baram, J. (1987). Evidence for direct inhibition of de novo purine synthesis in human MCF-7 breast cells as a principal mode of metabolic inhibition by methotrexate. J. Biol. Chem. *262*, 13520–13526.

Bruce, K.D., Cagampang, F.R., Argenton, M., Zhang, J., Ethirajan, P.L., Burdge, G.C., Bateman, A.C., Clough, G.F., Poston, L., Hanson, M.A., et al. (2009). Maternal high-fat feeding primes steatohepatitis in adult mice offspring, involving mitochondrial dysfunction and altered lipogenesis gene expression. Hepatology *50*, 1796–1808.

Carling, D., Clarke, P.R., Zammit, V.A., and Hardie, D.G. (1989). Purification and characterization of the AMP-activated protein kinase. Copurification of acetyl-CoA carboxylase kinase and 3-hydroxy-3-methylglutaryl-CoA reductase kinase activities. Eur. J. Biochem. *186*, 129–136.

Cheong, J.H., Park, E.S., Liang, J., Dennison, J.B., Tsavachidou, D., Nguyen-Charles, C., Wa Cheng, K., Hall, H., Zhang, D., Lu, Y., et al. (2011). Dual inhibition of tumor energy pathway by 2-deoxyglucose and metformin is effective against a broad spectrum of preclinical cancer models. Mol. Cancer Ther. *10*, 2350–2362.

Corton, J.M., Gillespie, J.G., and Hardie, D.G. (1994). Role of the AMP-activated protein kinase in the cellular stress response. Curr. Biol. *4*, 315–324.

Corton, J.M., Gillespie, J.G., Hawley, S.A., and Hardie, D.G. (1995). 5-aminoimidazole-4-carboxamide ribonucleoside. A specific method for activating AMP-activated protein kinase in intact cells? Eur. J. Biochem. *229*, 558–565.

Desharnais, J., Hwang, I., Zhang, Y., Tavassoli, A., Baboval, J., Benkovic, S.J., Wilson, I.A., and Boger, D.L. (2003). Design, synthesis and biological evaluation of 10-CF3CO-DDACTHF analogues and derivatives as inhibitors of GAR Tfase and the de novo purine biosynthetic pathway. Bioorg. Med. Chem. *11*, 4511–4521.

Ferrer, A., Caelles, C., Massot, N., and Hegardt, F.G. (1985). Activation of rat liver cytosolic 3-hydroxy-3-methylglutaryl coenzyme A reductase kinase by adenosine 5′-monophosphate. Biochem. Biophys. Res. Commun. *132*, 497–504.

Fullerton, M.D., Galic, S., Marcinko, K., Sikkema, S., Pulinilkunnil, T., Chen, Z.P., O'Neill, H.M., Ford, R.J., Palanivel, R., O'Brien, M., et al. (2013). Single phosphorylation sites in Acc1 and Acc2 regulate lipid homeostasis and the insulin-sensitizing effects of metformin. Nat. Med. *19*, 1649–1654.

Goodpaster, B.H., Katsiaras, A., and Kelley, D.E. (2003). Enhanced fat oxidation through physical activity is associated with improvements in insulin sensitivity in obesity. Diabetes *52*, 2191–2197.

Goodyear, L.J. (2008). The exercise pill—too good to be true? N. Engl. J. Med. *359*, 1842–1844.

Greasley, S.E., Horton, P., Ramcharan, J., Beardsley, G.P., Benkovic, S.J., and Wilson, I.A. (2001). Crystal structure of a bifunctional transformylase and cyclohydrolase enzyme in purine biosynthesis. Nat. Struct. Biol. *8*, 402–406.

Hardie, D.G. (2011a). AMP-activated protein kinase: a cellular energy sensor with a key role in metabolic disorders and in cancer. Biochem. Soc. Trans. *39*, 1–13.

Hardie, D.G. (2011b). AMP-activated protein kinase: an energy sensor that regulates all aspects of cell function. Genes Dev. *25*, 1895–1908.

Hardie, D.G., Scott, J.W., Pan, D.A., and Hudson, E.R. (2003). Management of cellular energy by the AMP-activated protein kinase system. FEBS Lett. *546*, 113–120.

Hawley, S.A., Davison, M., Woods, A., Davies, S.P., Beri, R.K., Carling, D., and Hardie, D.G. (1996). Characterization of the AMP-activated protein kinase kinase from rat liver and identification of threonine 172 as the major site at which it phosphorylates AMP-activated protein kinase. J. Biol. Chem. *271*, 27879–27887.

Hawley, S.A., Gadalla, A.E., Olsen, G.S., and Hardie, D.G. (2002). The antidiabetic drug metformin activates the AMP-activated protein kinase cascade via an adenine nucleotide-independent mechanism. Diabetes *51*, 2420–2425.

Henderson, J.F., and Khoo, K.Y. (1965). On the mechanism of feedback inhibition of purine biosynthesis de novo in Ehrlich ascites tumor cells in vitro. J. Biol. Chem. *240*, 3104–3109.

Jager, S., Handschin, C., St-Pierre, J., and Spiegelman, B.M. (2007). AMP-activated protein kinase (AMPK) action in skeletal muscle via direct phosphorylation of PGC-1alpha. Proc. Natl. Acad. Sci. USA *104*, 12017–12022.

Kahn, B.B., Alquier, T., Carling, D., and Hardie, D.G. (2005). AMP-activated protein kinase: ancient energy gauge provides clues to modern understanding of metabolism. Cell Metab. *1*, 15–25.

Karagounis, L.G., and Hawley, J.A. (2009). The 5′ adenosine monophosphate-activated protein kinase: regulating the ebb and flow of cellular energetics. Int. J. Biochem. Cell Biol. *41*, 2360–2363.

Liang, J., and Mills, G.B. (2013). AMPK: a contextual oncogene or tumor suppressor? Cancer Res. *73*, 2929–2935.

Marsilje, T.H., Labroli, M.A., Hedrick, M.P., Jin, Q., Desharnais, J., Baker, S.J., Gooljarsingh, L.T., Ramcharan, J., Tavassoli, A., Zhang, Y., et al. (2002). 10-Formyl-5,10-dideaza-acyclic-5,6,7,8-tetrahydrofolic acid (10-formyl-DDACTHF): a potent cytotoxic agent acting by selective inhibition of human GAR Tfase and the de novo purine biosynthetic pathway. Bioorg. Med. Chem. *10*, 2739–2749.

Marsilje, T.H., Hedrick, M.P., Desharnais, J., Tavassoli, A., Zhang, Y., Wilson, I.A., Benkovic, S.J., and Boger, D.L. (2003). Design, synthesis, and biological evaluation of simplified alpha-keto heterocycle, trifluoromethyl ketone, and formyl substituted folate analogues as potential inhibitors of GAR transformylase and AICAR transformylase. Bioorg. Med. Chem. *11*, 4487–4501.

Mayer, F.V., Heath, R., Underwood, E., Sanders, M.J., Carmena, D., McCartney, R.R., Leiper, F.C., Xiao, B., Jing, C., Walker, P.A., et al. (2011). ADP regulates SNF1, the *Saccharomyces cerevisiae* homolog of AMP-activated protein kinase. Cell Metab. *14*, 707–714.

Mitchelhill, K.I., Michell, B.J., House, C.M., Stapleton, D., Dyck, J., Gamble, J., Ullrich, C., Witters, L.A., and Kemp, B.E. (1997). Posttranslational modifications of the 5′-AMP-activated protein kinase beta1 subunit. J. Biol. Chem. *272*, 24475–24479.

Munday, M.R., Campbell, D.G., Carling, D., and Hardie, D.G. (1988). Identification by amino acid sequencing of three major regulatory phosphorylation sites on rat acetyl-CoA carboxylase. Eur. J. Biochem. *175*, 331–338.

Murray, A.W. (1971). The biological significance of purine salvage. Annu. Rev. Biochem. *40*, 811–826.

Narkar, V.A., Downes, M., Yu, R.T., Embler, E., Wang, Y.X., Banayo, E., Mihaylova, M.M., Nelson, M.C., Zou, Y., Juguilon, H., et al. (2008). AMPK and PPARdelta agonists are exercise mimetics. Cell *134*, 405–415.

Ni, L., Guan, K., Zalkin, H., and Dixon, J.E. (1991). De novo purine nucleotide biosynthesis: cloning, sequencing and expression of a chicken PurH cDNA encoding 5-aminoimidazole-4-carboxamide-ribonucleotide transformylase-IMP cyclohydrolase. Gene *106*, 197–205.

O'Neill, H.M., Lally, J.S., Galic, S., Thomas, M., Azizi, P.D., Fullerton, M.D., Smith, B.K., Pulinilkunnil, T., Chen, Z., Samaan, M.C., et al. (2014). AMPK phosphorylation of ACC2 is required for skeletal muscle fatty acid oxidation and insulin sensitivity in mice. Diabetologia *57*, 1693–1702.

Page, K., and Lange, Y. (1997). Cell adhesion to fibronectin regulates membrane lipid biosynthesis through 5′-AMP-activated protein kinase. J. Biol. Chem. *272*, 19339–19342.

Pinson, B., Vaur, S., Sagot, I., Coulpier, F., Lemoine, S., and Daignan-Fornier, B. (2009). Metabolic intermediates selectively stimulate transcription factor interaction and modulate phosphate and purine pathways. Genes Dev. *23*, 1399–1407.

Racanelli, A.C., Rothbart, S.B., Heyer, C.L., and Moran, R.G. (2009). Therapeutics by cytotoxic metabolite accumulation: pemetrexed causes ZMP accumulation, AMPK activation, and mammalian target of rapamycin inhibition. Cancer Res. *69*, 5467–5474.

Rattan, R., Giri, S., Singh, A.K., and Singh, I. (2005). 5-Aminoimidazole-4-carboxamide-1-beta-D-ribofuranoside inhibits cancer cell proliferation in vitro and in vivo via AMP-activated protein kinase. J. Biol. Chem. *280*, 39582–39593.

Rebora, K., Laloo, B., and Daignan-Fornier, B. (2005). Revisiting purine-histidine cross-pathway regulation in *Saccharomyces cerevisiae*: a central role for a small molecule. Genetics *170*, 61–70.

Rothbart, S.B., Racanelli, A.C., and Moran, R.G. (2010). Pemetrexed indirectly activates the metabolic kinase AMPK in human carcinomas. Cancer Res. *70*, 10299–10309.

Ruderman, N.B., Carling, D., Prentki, M., and Cacicedo, J.M. (2013). AMPK, insulin resistance, and the metabolic syndrome. J. Clin. Invest. *123*, 2764–2772.

Sengupta, T.K., Leclerc, G.M., Hsieh-Kinser, T.T., Leclerc, G.J., Singh, I., and Barredo, J.C. (2007). Cytotoxic effect of 5-aminoimidazole-4-carboxamide-1-beta-4-ribofuranoside (AICAR) on childhood acute lymphoblastic leukemia (ALL) cells: implication for targeted therapy. Mol. Cancer *6*, 46.

Shaw, R.J., Lamia, K.A., Vasquez, D., Koo, S.H., Bardeesy, N., Depinho, R.A., Montminy, M., and Cantley, L.C. (2005). The kinase LKB1 mediates glucose homeostasis in liver and therapeutic effects of metformin. Science *310*, 1642–1646.

Shih, C., Chen, V.J., Gossett, L.S., Gates, S.B., MacKellar, W.C., Habeck, L.L., Shackelford, K.A., Mendelsohn, L.G., Soose, D.J., Patel, V.F., et al. (1997). LY231514, a pyrrolo[2,3-d]pyrimidine-based antifolate that inhibits multiple folate-requiring enzymes. Cancer Res. *57*, 1116–1123.

Spurr, I.B., Birts, C.N., Cuda, F., Benkovic, S.J., Blaydes, J.P., and Tavassoli, A. (2012). Targeting tumour proliferation with a small-molecule inhibitor of AICAR transformylase homodimerization. Chembiochem *13*, 1628–1634.

Steinberg, G.R., and Kemp, B.E. (2009). AMPK in health and disease. Physiol. Rev. *89*, 1025–1078.

Su, R.Y., Chao, Y., Chen, T.Y., Huang, D.Y., and Lin, W.W. (2007). 5-Aminoimidazole-4-carboxamide riboside sensitizes TRAIL- and TNF{alpha}-induced cytotoxicity in colon cancer cells through AMP-activated protein kinase signaling. Mol. Cancer Ther. *6*, 1562–1571.

Tavassoli, A., and Benkovic, S.J. (2005). Genetically selected cyclic-peptide inhibitors of AICAR transformylase homodimerization. Angew. Chem. Int. Ed. Engl. *44*, 2760–2763.

Tsou, P., Zheng, B., Hsu, C.H., Sasaki, A.T., and Cantley, L.C. (2011). A fluorescent reporter of AMPK activity and cellular energy stress. Cell Metab. *13*, 476–486.

Vainer, G.W., Saada, A., Kania-Almog, J., Amartely, A., Bar-Tana, J., and Hertz, R. (2014). PF-4708671 activates AMPK independently of p70S6K1 inhibition. PLoS One *9*, e107364.

Van Den Neste, E., Van den Berghe, G., and Bontemps, F. (2010). AICA-riboside (acadesine), an activator of AMP-activated protein kinase with potential for application in hematologic malignancies. Expert Opin. Investig. Drugs *19*, 571–578.

Vila-Bedmar, R., Lorenzo, M., and Fernandez-Veledo, S. (2010). Adenosine 5′-monophosphate-activated protein kinase-mammalian target of rapamycin cross talk regulates brown adipocyte differentiation. Endocrinology *151*, 980–992.

Viollet, B., Foretz, M., Guigas, B., Horman, S., Dentin, R., Bertrand, L., Hue, L., and Andreelli, F. (2006). Activation of AMP-activated protein kinase in the liver: a new strategy for the management of metabolic hepatic disorders. J. Physiol. *574*, 41–53.

Viollet, B., Guigas, B., Leclerc, J., Hebrard, S., Lantier, L., Mounier, R., Andreelli, F., and Foretz, M. (2009). AMP-activated protein kinase in the regulation of hepatic energy metabolism: from physiology to therapeutic perspectives. Acta Physiol. (Oxf.) *196*, 81–98.

Viollet, B., Horman, S., Leclerc, J., Lantier, L., Foretz, M., Billaud, M., Giri, S., and Andreelli, F. (2010). AMPK inhibition in health and disease. Crit. Rev. Biochem. Mol. Biol. *45*, 276–295.

Winder, W.W., and Hardie, D.G. (1996). Inactivation of acetyl-CoA carboxylase and activation of AMP-activated protein kinase in muscle during exercise. Am. J. Physiol. *270*, E299–E304.

Xiao, B., Heath, R., Saiu, P., Leiper, F.C., Leone, P., Jing, C., Walker, P.A., Haire, L., Eccleston, J.F., Davis, C.T., et al. (2007). Structural basis for AMP binding to mammalian AMP-activated protein kinase. Nature *449*, 496–500.

Xiao, B., Sanders, M.J., Underwood, E., Heath, R., Mayer, F.V., Carmena, D., Jing, C., Walker, P.A., Eccleston, J.F., Haire, L.F., et al. (2011). Structure of mammalian AMPK and its regulation by ADP. Nature *472*, 230–233.

Yeh, L.A., Lee, K.H., and Kim, K.H. (1980). Regulation of rat liver acetyl-CoA carboxylase. Regulation of phosphorylation and inactivation of acetyl-CoA carboxylase by the adenylate energy charge. J. Biol. Chem. *255*, 2308–2314.

Zhang, B.B., Zhou, G., and Li, C. (2009). AMPK: an emerging drug target for diabetes and the metabolic syndrome. Cell Metab. *9*, 407–416.